Research Square

Preprints are preliminary reports that have not undergone peer review.
They should not be considered conclusive, used to inform clinical practice,
or referenced by the media as validated information.

Beyond Excitotoxicity: Glutamate-Independent Mechanisms Underlie Noise-Induced Synaptopathy and Compromise Gene Therapy for Hereditary Deafness

Xingle Zhao

2308985070@qq.com

Department of Otolaryngology Head and Neck Surgery, The First Affiliated Hospital of Zhengzhou University, Zhengzhou, China

Shuangshuang Lu

Wenxue Tang

Zhengzhou University https://orcid.org/0000-0001-8087-0900

Yueyu Wen

Jiake Zhao

Ying Cao

Jingjie Han

Jiali Wang

Jinming Yin

Haiyan Zhou

Hongen Xu

Zhengzhou University https://orcid.org/0000-0001-7895-0899

Mengli Zhang

Ling Tong

Changyun Yu

Article

Keywords: Noise, Hearing loss, Ribbon synapses, Glutamate, Vglut3, Gene Therapy

Posted Date: May 21st, 2026

DOI: https://doi.org/10.21203/rs.3.rs-9626899/v1

License: This work is licensed under a Creative Commons Attribution 4.0 International License.
Read Full License

Additional Declarations: There is **NO** Competing Interest.

Abstract

Noise-induced hearing loss (NIHL) is classically attributed to glutamate excitotoxicity, yet the precise requirement for synaptic glutamate release remains untested using genetic approaches. Here, we investigated noise-induced cochlear damage using *Vglut3* knockout (*Vglut3*-KO) mice, which lack glutamatergic transmission from inner hair cells. Following 116 dB SPL noise exposure, wild-type mice exhibited permanent threshold shifts, persistent ABR wave I amplitude reduction, and significant ribbon synapse loss at the 32 kHz region. Unexpectedly, *Vglut3*-KO mice also exhibited significant synapse loss despite their inability to release glutamate, revealing glutamate-independent mechanisms of synaptopathy. Proteomic analysis identified 62 differentially expressed proteins in noise-exposed cochleae, with significant enrichment in synaptic structures and extracellular matrix components, including up-regulation of *Rps6ka1*, *Cplx2*, and *Cdk5*, and downregulation of *Ppa2*. Importantly, noise exposure severely compromised AAV8-*Vglut3* gene therapy efficacy in *Vglut3*-KO mice: while unexposed mutants achieved complete functional recovery, noise-exposed animals failed to attain normal hearing thresholds. These findings demonstrate that high-intensity noise induces synaptopathy through both excitotoxic and non-excitotoxic mechanisms involving synaptic and ECM disruption, and that acoustic trauma creates persistent pathological changes limiting gene therapy outcomes, underscoring the need for comprehensive otoprotective strategies in hereditary deafness patients awaiting treatment.

Introduction

As the primary peripheral organ of the auditory system, the cochlea relies on the synaptic connections between inner hair cells and auditory nerve fibers—known as cochlear synapses—as the critical structures for auditory signal transmission[1]. The homeostasis of neurotransmitters is essential for maintaining normal synaptic function and ensuring efficient signal conduction[2]. Glutamate, the principal excitatory neurotransmitter at these synapses, facilitates auditory signal transmission under physiological conditions through its regulated release and clearance[2–4]. However, under pathological stress, dysregulation of glutamate release or impaired clearance leads to excitotoxicity. Excessive accumulation of glutamate overstimulates receptors on auditory nerve endings, triggering intracellular calcium overload and heightened oxidative stress[5]. These events subsequently cause neuronal damage and disruption of synaptic architecture. This mechanism has been identified as a central pathological process underlying various forms of auditory impairment, including noise-induced hearing loss (NIHL) and age-related degeneration[5].

Apart from the use of steroids, there are presently no established or effective drug therapies for managing Noise-Induced Hearing Loss in a clinical setting[6]. Despite decades of research establishing the central role of excitotoxicity in cochlear pathology, therapeutic translation remains elusive. This knowledge gap underscores the critical need to fully elucidate the multifactorial mechanisms underlying NIHL, particularly those operating independently of classical excitotoxicity, to identify novel therapeutic targets and develop effective intervention strategies[6].

Noise-induced hearing loss is classically associated with glutamate excitotoxicity, wherein excessive neurotransmitter release from inner hair cells (IHCs) overstimulates postsynaptic auditory nerve terminals, leading to rapid swelling, vacuolization, and synaptic degeneration[7–9]. To further investigate the underlying mechanisms, we utilized mice with targeted deletion of vesicular glutamate transporter type 3 (*Vglut3*), encoded by the SLC17A8 gene[10]. *Vglut3* is essential for packaging glutamate into synaptic vesicles within IHCs; consequently, *Vglut3* knockout (*Vglut3*-KO) mice are profoundly deaf despite retaining morphologically normal ribbon synapses, intact basolateral ion channels including CaV1.3, and preserved outer hair cell function as evidenced by normal distortion product otoacoustic emissions (DPOAEs)[2,3]. These mice thus provide a unique model in which presynaptic machinery remains structurally intact but functionally silent with respect to glutamatergic transmission[11].

To investigate the role of glutamate release in noise-induced cochlear damage, we subjected WT and *Vglut3*-KO mice to controlled noise exposure. In WT mice, high-intensity noise induced permanent auditory deficits accompanied by significant ribbon synapse loss. Unexpectedly, *Vglut3*-KO mice also exhibited significant synapse loss following exposure, despite their inability to release glutamate from inner hair cells, revealing that glutamate-independent mechanisms—potentially involving mechanical stress, metabolic dysregulation, or inflammatory mediators—contribute to noise-induced synaptopathy. To explore these mechanisms, we performed proteomic analysis on cochlear extracts from noise-exposed WT mice, revealing significant dysregulation of proteins involved in synaptic function, mitochondrial metabolism, and cellular stress responses, including upregulation of *Rps6ka1*, *Cplx2*, and *Cdk5*, and downregulation of *Ppa2*. Building upon these observations, we investigated whether genetic restoration of *Vglut3* expression could reverse noise-induced deficits. Despite successful functional recovery in unexposed *Vglut3*-KO controls following gene therapy, noise-exposed *Vglut3*-KO animals failed to achieve normal hearing thresholds, indicating that noise-induced cochlear damage creates persistent pathological changes that limit therapeutic efficacy even after correction of the primary genetic defect. These findings carry significant clinical implications for hereditary deafness patients awaiting gene therapies, underscoring the importance of comprehensive otoprotective strategies and environmental noise management prior to therapeutic intervention.

Results

Noise Exposure Induces Temporary and Permanent Threshold Shifts in WT Mice

To evaluate the impact of noise on hearing, 4- to 6-week-old WT and *Vglut3*-KO mice were exposed to broadband noise (2–20 kHz) at 110 dB SPL or 116 dB SPL for 2 hours. Auditory brainstem response (ABR) thresholds were measured at 3 and 14 days post-exposure and compared to unexposed controls (Fig. 1, S1). In WT mice exposed to 110 dB noise, significant threshold shifts were observed at 11.31, 16, 22.63, and 32 kHz on day 3 (26.7 ± 2.4, 38.3 ± 4.2, 55.6 ± 4.4, and 63.3 ± 4.6 dB vs. 13.9 ± 1.1, 15.6 ± 1.0, 19.4 ± 1.3, and 33.9 ± 1.1 dB at 11.31, 16, 22.63, and 32 kHz, $p < 0.05$. two-way ANOVA, N = 9 and 9,

Fig. 1A). By day 14, thresholds had largely recovered except at 32 kHz ($p < 0.0001$. two-way ANOVA, N = 9 and 9, Fig. 1A). Analysis of ABR wave I at 22.63 kHz revealed a significant reduction in amplitude on day 3 post-exposure (3.04 ± 0.24 μV vs. 5.26 ± 0.42 μV at 90 dB, n = 9 and 9, two-way ANOVA, $p < 0.0001$, Fig. 1C), followed by partial recovery by day 14, with some intensities returning to WT levels. Additionally, wave I latencies were prolonged on day 3 but shortened by day 14 (Fig. 1E), indicating functional recovery of auditory nerve responses.

In the 116 dB SPL white noise exposure group, significant threshold elevations were observed across all tested frequencies(65.6 ± 3.4, 56.7 ± 3.5, 58.9 ± 2.2, 62.8 ± 2.4, 72.8 ± 3.1, and 82.8 ± 2.2 dB vs. 37.2 ± 1.5, 26.1 ± 1.4, 13.9 ± 1.1, 15.6 ± 1.0, 19.4 ± 1.3, and 33.9 ± 1.1 dB at 5.66, 8, 11.31, 16, 22.63, and 32 kHz, $p < 0.0001$. two-way ANOVA, N = 9 and 9, Fig. 1B). Although a partial recovery occurred over time, thresholds did not return to normal baseline levels, consistent with permanent threshold shift (PTS). Analysis of ABR wave I at 22.63 kHz revealed markedly reduced amplitudes (0.89 ± 0.36 μV vs. 5.26 ± 1.25 μV at 90 dB, n = 9 and 9, two-way ANOVA, $p < 0.0001$, Fig. 1D) and prolonged latencies (Fig. 1F) following noise exposure, with no significant improvement over the 14-day recovery period. These results indicate persistent dysfunction of auditory nerve activity after severe acoustic trauma. Notably, *Vglut3*-KO mice exhibited no detectable auditory responses either before or after noise exposure.

Hair Cell Survival After Noise Exposure

To assess potential hair cell loss following noise exposure, we immunostained whole-mount cochlear preparations with an anti-Myo7a antibody to label inner and outer hair cells. Confocal imaging was performed on cochlear whole mounts from each experimental group. Quantitative analysis of hair cells was conducted across all cochlear turns (Figs. 2A, 2B, 2I and 2J) and evaluated statistically using two-way ANOVA. In both WT and *Vglut3*-KO mice exposed to broadband noise at 110 dB SPL, no significant loss of inner or outer hair cells was observed in the apical, middle, or basal turns compared to unexposed controls (Fig. 2C - H). These findings suggest that the temporary threshold shifts observed at this exposure level are not associated with permanent structural damage to sensory hair cells, indicating that the functional deficits likely result from transient metabolic or synaptic disruption rather than hair cell degeneration.

In WT and *Vglut3*-KO mice exposed to 116 dB SPL broadband noise, immunofluorescence staining for Myo7a revealed no significant loss of inner hair cells in the apical, middle, or basal cochlear turns compared to unexposed controls (Figs. 2K-P). However, scattered loss of outer hair cells was observed, predominantly in the basal turns(Figs. 2I - J). Despite this morphological pattern, quantitative analysis showed that outer hair cell survival rates in these regions did not reach statistical significance when compared to controls ($P > 0.05$). These findings suggest that while 116 dB noise exposure may induce focal outer hair cell damage, the extent of loss was limited and variable, resulting in non-significant quantitative differences. This partial outer hair cell loss may contribute to the observed auditory functional deficits without widespread structural destruction.

Noise-Induced Synaptopathy in WT and Vglut3-KO Mice

To investigate whether permanent threshold shift following 116 dB noise exposure involves synaptic damage, we immunostained cochlear whole mounts for CtBP2 to label presynaptic ribbons in inner hair cells. In wild-type mice, quantitative analysis at the 32 kHz region of the cochlea revealed a significant reduction in the number of ribbon synapses at 3 days post-exposure compared to unexposed controls (5.2 ± 1.1 vs. 17.3 ± 2.1, n = 9 and 7, one-way ANOVA, $p < 0.0001$). This reduction persisted at 14 days post-exposure (4.3 ± 2.2, n = 9), with no evidence of recovery (Figs. 3C, F). The sustained loss of ribbon synapses closely paralleled the permanent reduction in ABR wave I amplitude observed in vivo, suggesting that noise-induced excitotoxicity leads to irreversible synaptic damage. In contrast, quantitative analysis at the 16 kHz region of the cochlea showed no significant reduction in the number of ribbon synapses at 3 days post-exposure compared to unexposed controls (15.1 ± 1.9 vs. 14.8 ± 1.9, n = 12 and 12, one-way ANOVA, $p > 0.05$). These findings indicate that synaptopathy contributes to the functional deficits underlying permanent threshold shift, even in the absence of significant hair cell loss.

We compared ribbon synapse counts at middle (16 kHz) and basal (32 kHz) cochlear regions in 4- to 6-week-old unexposed WT and *Vglut3* - KO mice. In WT controls, inner hair cells (IHCs) contained approximately 15 ribbon synapses per cell at both locations (Fig. 2A). Consistent with our previous findings, unexposed Vglut - KO IHCs exhibited fewer ribbon synapses at both frequencies. Following exposure to 116 dB SPL noise, WT mice showed a significant reduction in synapse number at the 32 kHz region, with no recovery by day 14. Unexpectedly, *Vglut3* - KO mice also exhibited significant synapse loss at 32 kHz post-exposure (6.5 ± 1.0 vs. 11.7 ± 1.0, n = 12 and 9, one-way ANOVA, $p < 0.0001$), despite their inability to release glutamate from IHCs. In contrast, no significant changes in synapse density were observed at the 16 kHz region in *Vglut3*-KO mice following noise exposure. These findings reveal that glutamate-independent mechanisms—such as mechanical stress, metabolic dysregulation, or inflammatory responses—contribute to noise-induced synaptopathy. The absence of complete synaptic protection in *Vglut3*-KO mice suggests that high-intensity noise can directly damage presynaptic structures or activate alternative degenerative pathways, highlighting the multifactorial nature of cochlear injury following acoustic trauma.

Proteomic Profiling Reveals Synaptic and Extracellular Matrix Disruption After Noise Exposure

To investigate glutamate-independent mechanisms of noise-induced cochlear damage, we conducted quantitative mass spectrometry-based proteomic analysis of cochlear extracts from wild-type mice subjected to 116 dB SPL noise exposure. The proteomic dataset met stringent quality control metrics, with the majority of identified peptides being 7–20 amino acids in length and carrying 2–3 charges, consistent with typical tryptic digestion and MS/MS fragmentation (Figure S2A). Most proteins were quantified with two or more unique peptides, ensuring reliable identification and accurate quantification

(Figure S2B). Furthermore, the identified proteins spanned a broad and uniform molecular weight range, indicating no systematic bias in protein extraction or detection (Figure S2C).

Comparative analysis identified 62 differentially expressed proteins (DEPs) post-exposure, with 23 significantly upregulated and 39 downregulated (Fig. 4A). Notably, several proteins with established synaptic functions were altered, including upregulation of ribosomal protein S6 kinase alpha-1 (*Rps6ka1*), a kinase involved in synaptic plasticity and stress response; complexin-2 (*Cplx2*), a regulator of synaptic vesicle exocytosis; and cyclin-dependent kinase 5 (*Cdk5*), which modulates synaptic function and neuronal survival. Conversely, inorganic pyrophosphatase 2 (*Ppa2*), an enzyme critical for mitochondrial energy metabolism, was markedly downregulated. These proteomic findings were validated by quantitative PCR, confirming consistent transcriptional changes (Fig. 4G).

Gene Ontology (GO) enrichment analysis of cellular components revealed that DEPs were most significantly enriched in synaptic structures, including "synapse," "postsynapse," and "postsynaptic density" (Fig. 4B). Strikingly, parallel enrichment was observed for extracellular matrix (ECM) components, such as "collagen-containing extracellular matrix," "basement membrane," and "laminin complex," which play crucial roles in synapse formation, stabilization, and perisynaptic microenvironment maintenance[12]. The concurrent enrichment of both synaptic and ECM categories suggests that noise exposure induces a broader perturbation of the synaptic microenvironment beyond direct neuronal injury.

To further explore biological significance, we conducted GO molecular function enrichment analysis (Fig. 4D). We observed significant enrichment of functions directly relevant to synaptic signaling and neuronal physiology. Terms including angiotensin receptor binding and type 1 angiotensin receptor binding were significantly enriched, suggesting a potential role for the brain renin-angiotensin system in auditory processing. Enrichment of glycosphingolipid binding and sphingolipid binding points to possible noise-induced alterations in synaptic membrane composition, as these lipids are critical for synapse formation and stabilization. Notably, neurexin family protein binding was enriched—a key finding given that neurexins are essential presynaptic cell adhesion molecules mediating trans-synaptic interactions fundamental for synapse specification and function[13,14]. Additionally, enrichment of growth factor activity and fibroblast growth factor binding suggests that neurotrophic signaling pathways, crucial for neuronal survival and synaptic plasticity, are differentially regulated following noise exposure.

KEGG pathway analysis (Fig. 4E) demonstrated that DEPs were distributed across five KEGG Level 1 categories. Within the Organismal Systems category, DEPs were annotated to "Nervous system" (5 proteins) and "Sensory system" (3 proteins), directly implicating neuronal and sensory pathways. The detection of DEPs in "Transport and catabolism" (6 proteins) and "Cellular community - eukaryotes" (5 proteins) within the Cellular Processes category further supports the hypothesis of noise-induced disruption to intercellular communication and synaptic microenvironments.

Reactome pathway enrichment analysis (Fig. 4F) revealed robust and highly significant enrichment of pathways related to ECM organization and remodeling, including "Extracellular matrix organization," "Collagen formation," and "Collagen degradation." Beyond ECM-related pathways, we identified significant enrichment of key signaling cascades relevant to neuronal function and synaptic plasticity, including "Signaling by Receptor Tyrosine Kinases," "Signaling by GPCR," and "GPCR downstream signalling." Pathways involved in cell adhesion and motility, such as "MET promotes cell motility" and "MET activates PTK2 signaling," were also enriched. The enrichment of "Signaling by NOTCH" and "Activation of SMO" points to potential involvement of developmental pathways in the cochlear response to noise-induced damage. Collectively, these findings demonstrate that noise exposure profoundly impacts synaptic structures, ECM organization, and multiple signaling cascades governing synaptic function and intercellular communication. The concurrent disruption of synaptic proteins and their perisynaptic ECM microenvironment provides compelling evidence for non-excitotoxic mechanisms underlying cochlear synaptopathy, highlighting the intricate relationship between synaptic integrity and extracellular matrix homeostasis in auditory processing.

Proteomic Profiling of Vglut3 Knockout Mice Reveals Extensive Synaptic and Metabolic Alterations

To dissect glutamate-dependent versus independent mechanisms in cochlear synaptic physiology, we performed comparative proteomic analysis of cochlear extracts from WT and *Vglut3* knockout mice. *Vglut3* is essential for glutamatergic transmission at inner hair cell synapses, and its deletion serves as a model for examining the consequences of disrupted synaptic signaling. Comparative analysis identified 233 differentially expressed proteins (DEPs) in *Vglut3*-KO mice relative to WT controls, with only 3 significantly upregulated and 230 downregulated, as visualized by volcano plot (Fig. 5A). The striking predominance of downregulated proteins suggests that loss of *Vglut3*-mediated glutamatergic transmission triggers widespread proteomic changes extending far beyond the immediate synaptic machinery. Hierarchical clustering analysis (Fig. 5B) demonstrated distinct separation between WT and *Vglut3*-KO samples.

Gene Ontology (GO) enrichment analysis of cellular components revealed that DEPs in *Vglut3*-KO mice were most significantly enriched in synaptic structures, including "synapse," "postsynaptic density," and "presynaptic active zone" (Fig. 5C). Additionally, strong enrichment was observed for mitochondrial compartments, such as "mitochondrion" and "mitochondrial inner membrane," indicating that *Vglut3* deletion impacts energy metabolism. Extracellular matrix components, including "collagen-containing extracellular matrix" and "basement membrane," were also significantly enriched.

To further explore biological significance, we conducted GO molecular function enrichment analysis (Fig. 5D). We observed significant enrichment of functions directly relevant to synaptic transmission and neuronal physiology. Terms including "structural constituent of postsynaptic density" and "glutamate receptor binding" were significantly enriched, consistent with the role of *Vglut3* in glutamatergic signaling. Notably, enrichment of "voltage-gated ion channel activity" and "calcium channel activity" points to alterations in membrane excitability and calcium homeostasis. Enrichment of "ATPase activity"

and "electron transfer activity" further supports mitochondrial dysfunction, while "extracellular matrix structural constituent" enrichment confirms ECM involvement.

KEGG pathway analysis (Fig. 5E) demonstrated that DEPs in *Vglut3*-KO mice were predominantly distributed across multiple KEGG Level 1 categories. Within the Organismal Systems category, DEPs were strongly annotated to "Nervous system" (25 proteins) and "Sensory system" (18 proteins), directly implicating neuronal and auditory pathways. The detection of DEPs in "Transport and catabolism" (22 proteins) and "Cellular community - eukaryotes" (15 proteins) within the Cellular Processes category supports disruption of intercellular communication. Notably, significant representation in "Energy metabolism" (12 proteins) and "Amino acid metabolism" (10 proteins) within the Metabolism category confirms the metabolic consequences of *Vglut3* deletion.

WikiPathways enrichment analysis (Fig. 5F) revealed robust enrichment of pathways related to synaptic function and energy metabolism. Multiple synapse-associated pathways were significantly enriched, including "Postsynaptic density proteins," "Synaptic vesicle pathway," and "Glutamatergic synapse." Strikingly, numerous mitochondrial pathways emerged as highly enriched, including "Electron transport chain," "Oxidative phosphorylation," and "Mitochondrial complex I assembly," indicating profound metabolic remodeling. Pathways related to "GABAergic synapse" and "Dopaminergic synapse" were also enriched, suggesting that loss of *Vglut3*-mediated signaling triggers compensatory changes in other neurotransmitter systems. Additionally, "ECM-receptor interaction" and "Focal adhesion" pathways were enriched, further supporting ECM involvement. Collectively, these findings demonstrate that genetic deletion of *Vglut3*, a core component of glutamatergic transmission at auditory synapses, induces extensive proteomic alterations encompassing synaptic structure, mitochondrial function, energy metabolism, and extracellular matrix organization.

Noise Exposure Compromises Gene Therapy Efficacy in Hereditary Deafness

Building upon our proteomic observations and the cochlear morphological changes (including inner hair cell ribbon synapses and outer hair cells) following noise exposure in *Vglut3*-KO mice, we next investigated whether inner ear gene therapy could restore auditory function in these animals following noise insult. As shown in Fig. 6, WT mice exhibited normal auditory responses (Fig. 6A), while untreated *Vglut3*-KO mice showed absent responses (Fig. 6B). Following AAV8-*Vglut3* gene therapy via posterior semicircular canal injection (PSCC), unexposed *Vglut3*-KO mice achieved restoration of auditory function (Fig. 6C). In contrast, WT mice exposed to 116 dB SPL broadband noise displayed reduced ABR waveforms 14 days post-exposure (Fig. 6D). Notably, when noise-exposed *Vglut3*-KO mice received the same gene therapy regimen and were assessed 14 days later, they failed to achieve comparable functional recovery (Fig. 6E).

Quantification of ABR thresholds across all tested frequencies confirmed that while unexposed *Vglut3*-KO mice achieved complete functional recovery following gene therapy (65.6 ± 3.4, 56.7 ± 3.5, 58.9 ± 2.2,

62.8 ± 2.4, 72.8 ± 3.1, and 82.8 ± 2.2 dB vs. 37.2 ± 1.5, 26.1 ± 1.4, 13.9 ± 1.1, 15.6 ± 1.0, 19.4 ± 1.3, and 33.9 ± 1.1 dB at 5.66, 8, 11.31, 16, 22.63, and 32 kHz, $p < 0.0001$. two-way ANOVA, N = 9 and 9, Fig. 6F), noise-exposed *Vglut3*-KO animals exhibited elevated thresholds (65.6 ± 3.4, 56.7 ± 3.5, 58.9 ± 2.2, 62.8 ± 2.4, 72.8 ± 3.1, and 82.8 ± 2.2 dB vs. 37.2 ± 1.5, 26.1 ± 1.4, 13.9 ± 1.1, 15.6 ± 1.0, 19.4 ± 1.3, and 33.9 ± 1.1 dB at 5.66, 8, 11.31, 16, 22.63, and 32 kHz, $p < 0.0001$. two-way ANOVA, N = 9 and 9, Fig. 6F). This incomplete rescue demonstrates that noise-induced cochlear damage creates persistent pathological changes that limit therapeutic efficacy even after correction of the primary genetic defect. The differential recovery between unexposed and noise-exposed cohorts indicates that noise exposure inflicts lasting structural and molecular alterations that cannot be overcome by genetic intervention alone. These findings carry significant clinical implications for patients with profound or severe hereditary deafness who are candidates for emerging gene therapies. Our results strongly suggest that such individuals should strictly avoid exposure to high-intensity noise prior to treatment, as noise-induced damage may permanently compromise therapeutic outcomes. The persistence of noise-induced pathology despite successful genetic intervention underscores the importance of comprehensive otoprotective counseling and environmental noise management in the clinical management of genetic deafness patients awaiting novel therapies.

Discussion

This study demonstrates that noise exposure induces both temporary and permanent auditory deficits in wild-type mice, with severity dependent on intensity. At 110 dB SPL, threshold shifts were largely reversible and not associated with hair cell loss, suggesting transient metabolic or synaptic disruption. In contrast, 116 dB SPL exposure caused permanent threshold shifts, persistent ABR wave I amplitude reduction, and significant ribbon synapse loss at the 32 kHz cochlear region, indicative of irreversible synaptopathy. Notably, *Vglut3*-KO mice also exhibited synapse loss despite lacking glutamate release, revealing glutamate-independent damage mechanisms. Proteomic profiling confirmed noise-induced disruption of synaptic proteins and extracellular matrix components. Importantly, noise exposure compromised AAV8-*Vglut3* gene therapy efficacy in *Vglut3*-KO mice, highlighting that acoustic trauma creates lasting pathological changes that limit therapeutic restoration, underscoring the need for noise protection in gene therapy candidates.

An unexpected and significant finding of our study is that *Vglut3*-KO mice exhibited significant ribbon synapse loss at the 32 kHz cochlear region following 116 dB SPL noise exposure, despite their inability to release glutamate from inner hair cells. This observation reveals that glutamate-independent mechanisms—such as mechanical stress, metabolic dysregulation, or inflammatory responses—contribute substantially to noise-induced synaptopathy. While previous studies using moderate-intensity noise (100 dB SPL) reported no statistically significant synapse loss in *Vglut3*-KO mice[15], potentially due to differences in exposure intensity, frequency range, or the cochlear regions analyzed, our higher-intensity broadband exposure likely engaged additional damage pathways that overcome the protection afforded by absent glutamate release. Notably, even in studies where synapse counts were preserved,

noise exposure consistently altered synaptic morphology in *Vglut3*-KO mice[15], including enlargement of presynaptic ribbons and postsynaptic AMPA receptor clusters, indicating that acoustic trauma induces structural synaptic changes independent of glutamatergic transmission. These findings highlight the multifactorial nature of cochlear injury following acoustic trauma and suggest that high-intensity noise can directly damage presynaptic structures or activate alternative degenerative pathways. The absence of complete synaptic protection in *Vglut3*-KO mice underscores that therapeutic strategies targeting only excitotoxicity may be insufficient to prevent noise-induced hearing loss, necessitating broader approaches that address mechanical, metabolic, and inflammatory components of cochlear injury.

To explore glutamate-independent mechanisms underlying noise-induced cochlear damage, we performed quantitative proteomic analysis of cochlear extracts from wild-type mice exposed to 116 dB SPL noise. We identified 62 differentially expressed proteins, with significant enrichment in synaptic structures and extracellular matrix components. Notably, proteins involved in synaptic function—including Rps6ka1[16], Cplx2[17], and Cdk5[18,19]—were upregulated, while Ppa2[20], critical for mitochondrial energy metabolism, was downregulated. Parallel enrichment of ECM categories such as collagen-containing matrix and laminin complexes indicates that noise exposure disrupts not only synaptic integrity but also the perisynaptic microenvironment essential for synapse stabilization. Molecular function analysis revealed enrichment of neurexin family protein binding, glycosphingolipid binding, and growth factor activity, implicating alterations in trans-synaptic adhesion, membrane composition, and neurotrophic signaling. Pathway analyses further confirmed robust ECM remodeling and disruption of signaling cascades governing neuronal function and intercellular communication. Collectively, these findings provide compelling evidence for non-excitotoxic mechanisms of cochlear synaptopathy, demonstrating that acoustic trauma induces broad perturbations to synaptic proteins and their extracellular microenvironment. The intricate relationship between synaptic integrity and ECM homeostasis highlighted here suggests that therapeutic strategies targeting excitotoxicity alone may be insufficient, necessitating broader approaches that address the multifactorial nature of noise-induced cochlear injury.

Our proteomic analysis revealed extensive downregulation of synaptic pathways in Vglut3-KO mice, including terms such as “synapse,” “postsynaptic density,” and “glutamate receptor binding.” These findings indicate that the absence of Vglut3-mediated glutamatergic transmission profoundly disrupts synaptic architecture and maintenance, consistent with the observed reduction in inner hair cell ribbon synapse counts in Vglut3-KO mice compared to wild-type controls (Fig. 3). The proteomic signature thus supports the notion that constitutive loss of glutamatergic signaling impairs synapse development and stability.The proteomic data further revealed that noise exposure in wild-type animals engages a broad range of pathways beyond glutamatergic signaling, including those involved in energy metabolism, oxidative stress response, and extracellular matrix remodeling. This suggests that noise-induced synaptopathy cannot be explained solely by glutamate excitotoxicity. Instead, our findings support a model in which noise-induced synaptic damage results from the convergence of glutamatergic mechanisms and additional contributing pathways.

Another critical finding of our study is that noise exposure severely compromises the efficacy of gene therapy for hereditary deafness. Even after successful correction of the primary genetic defect, noise-induced cochlear damage significantly limits the restoration of auditory function. To our knowledge, this is the first demonstration of a negative interaction between noise exposure and gene therapy outcomes in the inner ear. The underlying mechanisms likely involve multiple noise-induced cochlear pathologies. First, the significant reduction in ribbon synapses, particularly in the basal region following 116 dB SPL exposure, directly impairs synaptic transmission between inner hair cells and auditory nerve fibers, limiting information transfer even after *Vglut3* expression is restored. Second, the scattered loss of outer hair cells in middle and basal turns may compromise cochlear amplification, affecting auditory sensitivity. Third, previous studies have documented noise-induced demyelination of auditory nerve fibers and spiral ganglion neuron damage, which could permanently alter neural conduction properties and impair transmission of regenerated signals to central auditory targets[21,22].

Accumulating evidence suggests that the efficacy of gene therapy for hereditary deafness is highly dependent on the timing of intervention[23,24]. Clinical observations from Otof mutation patients indicate superior outcomes in children compared to adults[25–27], and animal studies demonstrate that therapeutic success diminishes with age due to progressive hair cell degeneration[28]. While most preclinical studies have focused on neonatal intervention[4,29–34], our findings extend this concept by demonstrating that therapeutic timing remains critical even in early adulthood: 5-week-old *Vglut3*-KO mice achieved complete functional recovery following gene therapy, whereas 20-week-old mice showed only partial improvement, underscoring the impact of cochlear structural integrity—particularly synaptic preservation—on therapeutic outcomes[35]. Building on these observations, we propose that genetic deafness patients awaiting gene therapy should strictly avoid high-intensity noise exposure, as noise-induced synaptopathy and microenvironmental alterations may permanently undermine therapeutic potential. By extension, any factors that damage cochlear structures—including ototoxic drugs, surgical trauma, infection, or ischemia-reperfusion injury—should be rigorously avoided, as they may compromise gene therapy outcomes through disruption of synaptic integrity, hair cell function, or neuronal survival. These findings have important implications for the clinical management of genetic deafness, suggesting that comprehensive otoprotective strategies before and after gene therapy are essential to ensure optimal therapeutic outcomes.

Despite these important findings, several limitations of our study should be acknowledged. First, our analysis of noise-induced synaptopathy focused primarily on presynaptic ribbon counts using CtBP2 labeling, without concomitant assessment of postsynaptic AMPA receptor patches. Simultaneous evaluation of both pre- and postsynaptic elements would provide a more comprehensive understanding of synaptic integrity and enable distinction between true synapse loss versus simple uncoupling of paired synaptic structures. Second, while our proteomic profiling revealed compelling alterations in synaptic and extracellular matrix proteins following noise exposure, these findings represent primarily descriptive observations. Further mechanistic studies—including genetic or pharmacological manipulations of candidate pathways such as neurexin signaling, ECM remodeling, or mitochondrial

function—are needed to establish causal relationships with observed synaptic pathology. Third, although we demonstrated that noise exposure compromises gene therapy efficacy in *Vglut3*-KO mice, validation in additional deafness models with distinct genetic etiologies will be essential to establish the generalizability of this phenomenon. Nevertheless, our study provides critical evidence that noise-induced cochlear damage extends beyond excitotoxicity to encompass broader synaptic and extracellular matrix disruption, and that such pathological changes can permanently undermine therapeutic outcomes even after successful genetic correction. These findings underscore the importance of comprehensive otoprotective strategies for gene therapy candidates and open new avenues for investigating multifactorial mechanisms of cochlear injury.

Materials and Methods

Animal models

All animals were housed in accredited barrier facilities with controlled environmental conditions and received standardized access to food and water. This study received ethical approval from the Institutional Animal Care and Use Committee of the First Affiliated Hospital of Zhengzhou University (Henan, China). Male C57BL/6J mice (aged 4–6 weeks) were obtained from GemPharmatech Co., Ltd. (Nanjing, China), and *Vglut3* knockout (*Vglut3*-KO) mice were provided by the Institute of Neuroscience, CAS Center for Excellence in Brain Science and Intelligence Technology, Shanghai Institutes for Biological Sciences, Chinese Academy of Sciences[36]. All experimental procedures were performed in full compliance with the 3Rs principles of animal research—Reduction, Replacement, and Refinement. Mice of the same genotype were randomly assigned to experimental groups according to the study design. They were housed under a 12-hour light/dark cycle with free access to food and water throughout the experiment.

Acoustic exposure

Acoustic overexposure was conducted within a calibrated reverberant chamber characterized by minimal spatial variation in sound pressure level (approximately ± 1 dB across typical specimen locations). Broadband noise (2–20 kHz frequency range) was generated using a Tucker-Davis Technologies RZ6 audio processor and amplified through a Yamaha power amplifier coupled to a loudspeaker. Prior to each exposure session, the sound field was calibrated to the target intensity (110 dB SPL or 116 dB SPL) positioned at the level of the animal's ears. Unanesthetized mice were then placed in the chamber and exposed to the continuous bandpass noise for a duration of 2 hours. To ensure uniformity of exposure across all subjects, animals were confined to a small wire cage within the calibrated zone, and the sound pressure level was verified at multiple positions before and after each exposure session.

Auditory testing

Auditory brainstem responses (ABRs) were obtained from mice anesthetized with intraperitoneal chloral hydrate (480 mg/kg), with body temperature maintained at 37°C. Subdermal electrodes were placed at the vertex, mastoid, and tail base. Using Tucker-Davis Technologies hardware, 3-ms tone pips (1-ms ramp, 20 Hz) were presented. For each frequency and level, 400 responses were averaged via BioSigRZ software. Hearing thresholds were determined in 5-dB steps from 90 dB SPL (5.66–32 kHz). Wave I amplitude (peak-to-trough) and latency were measured to assess neural response. All recordings were conducted by a single experimenter.

Immunohistochemistry

Adult mouse cochleae were collected and fixed by intralabyrinthine perfusion with 4% paraformaldehyde, followed by decalcification in 120 mM EDTA (pH 7.4) for 3–4 hours. Following microdissection to expose the organ of Corti, the sensory epithelia were processed as whole-mount preparations. For immunolabeling, tissues were blocked with 5% blocking buffer (1 hour, room temperature) and then incubated overnight at 4℃ with primary antibodies against Myo7A (1:300, Proteus Biosciences) for hair cell identification and Ctbp2 (1:200, BD Biosciences) for presynaptic ribbon visualization. After three PBS washes, specimens were incubated for 1 hour with Alexa Fluor-conjugated secondary antibodies (1:500, Invitrogen). Phalloidin (1:500, Abcam) was co-applied to stain F-actin-rich structures. Confocal z-stacks were captured using a Zeiss LSM 880 microscope equipped with 20× and 63× glycerin-immersion objectives. Image stacks were then used to generate tonotopic maps via an ImageJ plugin, enabling quantitative analysis along the cochlear spiral.

Mass spectrometry-based proteomics and data analysis

To compare cochlear protein expression profiles before and after noise exposure, the organ of Corti from 4–6 week-old wild-type mice was harvested and lysed in ice-cold RIPA buffer supplemented with protease and phosphatase inhibitors (Thermo Fisher Scientific). Protein lysates (200 μg) were reduced with DTT, alkylated with iodoacetamide, and digested overnight with trypsin (1:40, w/w) at 37°C. The resulting peptides were fractionated into 24 fractions by basic reversed-phase liquid chromatography on an Ultimate 3000 system equipped with an XBridge C18 column (4.6 mm × 250 mm, 5 μm; Waters). Each fraction was vacuum-dried and subsequently analyzed by nanoLC-MS/MS using an EASY-nanoLC 1200 system coupled to an Orbitrap Fusion Lumos Tribrid mass spectrometer (Thermo Fisher Scientific). Peptides were separated on an Acclaim PepMap C18 column (75 μm × 25 cm) with a 60-min gradient at 400 nL/min (solvent A: 0.1% formic acid in water; solvent B: 0.1% formic acid in 80% ACN). The mass spectrometer was operated in data-independent acquisition (DIA) mode with automatic switching between MS and MS/MS. Raw data were searched against the UniProt database for protein identification. Quantitative analysis, including assessment of abundance distribution and reproducibility, was subsequently performed.

RT-qPCR

Cochlear tissues (50 mg) were homogenized in TRIzol reagent (Thermo, 15596-018CN) using a cryogenic grinder. Total RNA was extracted with chloroform, precipitated with isopropanol, washed with

75% ethanol, and dissolved in DEPC-treated water. RNA concentration was measured using a NanoDrop spectrophotometer. One microgram of purified RNA was used to prepare a 20 μL reverse transcription reaction system following the instructions of the SPARKscript II All-in-one RT SuperMix kit (Sparkjade, AG0305-B). Reverse transcription was performed in a 96-well PCR thermal cycler (Applied Biosystems, 4375786) under the following conditions: 50°C for 15 minutes, followed by 80°C for 5 seconds, to obtain cDNA. Real-time fluorescent quantitative PCR was performed on an Archimed X4 system using SGExcel FastSYBR Master Mix (Sangon, B532955), gene-specific primers, 2 μL of template cDNA, and ddH_2O in a 20 μL reaction system. The thermal cycling conditions were: 95°C for 30 sec, followed by 40 cycles of 95°C for 5 sec and 60°C for 30 sec. Melt curve analysis was performed to verify primer specificity. Relative gene expression was calculated using the 2^(-ΔΔCt) method with appropriate housekeeping genes as internal controls. Each sample was analyzed in triplicate, and non-template controls were included.

Production of virus

For this study, we utilized adeno-associated virus serotype 8 (AAV8) vectors encoding *Vglut3*-FLAG under the control of a cytomegalovirus (CMV) promoter. These viral constructs were generated and supplied by ViGene Biosciences, a company based in Shandong, China. The working stock of AAV8-*Vglut3*-FLAG was adjusted to a concentration of 2.04×10^{13} genome copies/mL prior to experimental use.

Microinjection into the inner ear of adult mice

To deliver AAV into the posterior semicircular canal (PSCC), 4-week-old mice were anesthetized with intraperitoneal 5% chloral hydrate. A postauricular incision was made, and the PSCC was visualized after separating the pinna and sternocleidomastoid muscle. The canal was perforated with a Bonn microprobe, and a glass micropipette connected to a Nanoliter 2000 injector was inserted and sealed with tissue adhesive. A total of 1 μL of viral solution was infused at 169 nL/min. After injection, the tubing was trimmed, sealed, and the incision was closed with 7/0 sutures.

Statistical analysis

All statistical analyses were performed with GraphPad Prism (USA). Differences between groups were evaluated using one-way or two-way ANOVA, with Bonferroni post hoc correction. Statistical significance was defined as $p < 0.05$. Data are expressed as mean ± SD in the text and as mean ± SEM in the figures. Significance levels are indicated as: *$p < 0.05$, **$p < 0.01$, ***$p < 0.001$, ****$p < 0.0001$; NS denotes not significant ($p > 0.05$).

Declarations

Declaration of Interests

This manuscript represents original work that has not been previously published, in whole or in part, and is not under consideration for publication by any other journal. All content presented herein is original,

with no text or data reproduced from previously published sources without proper attribution. Each author has reviewed and endorsed the final submitted version, and the authors declare that they have no competing interests associated with this submission.

Consent for publication

Written informed consent for publication was obtained from all participants.

Author contributions

C.Y. initiated and managed the project, while S.L. and X.Z. conceived and designed the experiments. X.Z., L.T. and M.Z. performed most of the experiments and data analysis. All authors contributed to data analysis, interpretation, and presentation. X.Z. wrote the manuscript with contributions from all authors.

Acknowledgements

This work was supported by the National Natural Science Foundation of China (No. 82501427), the National Natural Science Foundation of China (No. 82371160), the National Natural Science Foundation of Henan Province (No. 252300423920), the China Postdoctoral Science Foundation (No. 2024M752977), the Medical Science and Technology Research Plan Joint Construction Project of Henan Province (No. LHGJ20240279), the Discipline Cultivation Project of the First Affiliated Hospital of Zhengzhou University(2025XKPY002) and the Postdoctoral Research Foundation of the First Affiliated Hospital of Zhengzhou University (No. 72137).

We also thank the Precision Medicine Center, Academy of Medical Sciences, Zhengzhou University, and the Key Laboratory for Research on Deafness Mechanism, Henan Provincial Health Commission (Henan Health Science and Education Letter 2021, No. 44) for their support.

References

1. Moser, T., Starr, A.: Auditory neuropathy–neural and synaptic mechanisms. Nat. reviews Neurol. **12**, 135–149 (2016). 10.1038/nrneurol.2016.10
2. Ruel, J., et al.: Impairment of SLC17A8 encoding vesicular glutamate transporter-3, VGLUT3, underlies nonsyndromic deafness DFNA25 and inner hair cell dysfunction in null mice. Am. J. Hum. Genet. **83**, 278–292 (2008). 10.1016/j.ajhg.2008.07.008
3. Seal, R.P., et al.: Sensorineural deafness and seizures in mice lacking vesicular glutamate transporter 3. Neuron. **57**, 263–275 (2008). 10.1016/j.neuron.2007.11.032
4. Akil, O., et al.: Restoration of hearing in the VGLUT3 knockout mouse using virally mediated gene therapy. Neuron. **75**, 283–293 (2012). 10.1016/j.neuron.2012.05.019

5. Sebe, J.Y., et al.: Ca(2+)-Permeable AMPARs Mediate Glutamatergic Transmission and Excitotoxic Damage at the Hair Cell Ribbon Synapse. J. neuroscience: official J. Soc. Neurosci. **37**, 6162–6175 (2017). 10.1523/jneurosci.3644-16.2017
6. Xu, K., et al.: Intrinsic mechanism and pharmacologic treatments of noise-induced hearing loss. Theranostics. **13**, 3524–3549 (2023). 10.7150/thno.83383
7. Hakuba, N., Koga, K., Gyo, K., Usami, S.I., Tanaka, K.: Exacerbation of noise-induced hearing loss in mice lacking the glutamate transporter GLAST. J. neuroscience: official J. Soc. Neurosci. **20**, 8750–8753 (2000). 10.1523/jneurosci.20-23-08750.2000
8. Chen, Z., Peppi, M., Kujawa, S.G., Sewell, W.F.: Regulated expression of surface AMPA receptors reduces excitotoxicity in auditory neurons. J. Neurophysiol. **102**, 1152–1159 (2009). 10.1152/jn.00288.2009
9. Wang, L., Xu, M., Zhang, Q., Li, G.L.: Amitriptyline protects afferent synapses in the cochlea against excitotoxic trauma in vitro. FEBS J. **291**, 4111–4124 (2024). 10.1111/febs.17233
10. Zhao, X., et al.: Gene therapy restores auditory function and rescues damaged inner hair cells in an aged Vglut3 knockout mouse model. Gene Ther. (2025). 10.1038/s41434-025-00558-1
11. Zhang, T., et al.: Rapid cochlear gene therapy in adult deaf mice: Vglut3 rescue via AAV8 achieves day-1 hearing restoration. Mol. therapy Methods Clin. Dev. **33**, 101539 (2025). 10.1016/j.omtm.2025.101539
12. Zheng, G., Hu, B.H.: Cell-cell junctions: a target of acoustic overstimulation in the sensory epithelium of the cochlea. BMC Neurosci. **13**, 71 (2012). 10.1186/1471-2202-13-71
13. Li, T., et al.: The Neurexin/N-Ethylmaleimide-sensitive Factor (NSF) Interaction Regulates Short Term Synaptic Depression. J. Biol. Chem. **290**, 17656–17667 (2015). 10.1074/jbc.M115.644583
14. Tsetsenis, T., Boucard, A.A., Araç, D., Brunger, A.T., Südhof, T.C.: Direct visualization of trans-synaptic neurexin-neuroligin interactions during synapse formation. J. neuroscience: official J. Soc. Neurosci. **34**, 15083–15096 (2014). 10.1523/jneurosci.0348-14.2014
15. Kim, K.X., et al.: Vesicular Glutamatergic Transmission in Noise-Induced Loss and Repair of Cochlear Ribbon Synapses. J. neuroscience: official J. Soc. Neurosci. **39**, 4434–4447 (2019). 10.1523/jneurosci.2228-18.2019
16. Suzuki, T., Mitake, S., Murata, S.: Presence of up-stream and downstream components of a mitogen-activated protein kinase pathway in the PSD of the rat forebrain. Brain Res. **840**, 36–44 (1999). 10.1016/s0006-8993(99)01762-x
17. Vaithianathan, T., Henry, D., Akmentin, W., Matthews, G.: Functional roles of complexin in neurotransmitter release at ribbon synapses of mouse retinal bipolar neurons. J. neuroscience: official J. Soc. Neurosci. **35**, 4065–4070 (2015). 10.1523/jneurosci.2703-14.2015
18. Huang, H., et al.: Cdk5-dependent phosphorylation of liprinα1 mediates neuronal activity-dependent synapse development. Proc. Natl. Acad. Sci. U.S.A. **114**, E6992–e7001 (2017). 10.1073/pnas.1708240114

19. Zhai, X., Liu, C., Zhao, B., Wang, Y., Xu, Z.: Inactivation of Cyclin-Dependent Kinase 5 in Hair Cells Causes Hearing Loss in Mice. Front. Mol. Neurosci. **11**, 461 (2018). 10.3389/fnmol.2018.00461
20. Mishra, S.R., et al.: PPA2 activates MTFP1-DNM1L fission signaling to govern mitochondrial proliferation and mitophagy. Autophagy. **22**, 121–144 (2026). 10.1080/15548627.2025.2552900
21. Tagoe, T., Barker, M., Jones, A., Allcock, N., Hamann, M.: Auditory nerve perinodal dysmyelination in noise-induced hearing loss. J. neuroscience: official J. Soc. Neurosci. **34**, 2684–2688 (2014). 10.1523/jneurosci.3977-13.2014
22. Panganiban, C.H., et al.: Noise-Induced Dysregulation of Quaking RNA Binding Proteins Contributes to Auditory Nerve Demyelination and Hearing Loss. J. neuroscience: official J. Soc. Neurosci. **38**, 2551–2568 (2018). 10.1523/jneurosci.2487-17.2018
23. Lahlou, G., et al.: Extended time frame for restoring inner ear function through gene therapy in Usher1G preclinical model. JCI insight. **9** (2024). 10.1172/jci.insight.169504
24. Iizuka, T., et al.: Perinatal Gjb2 gene transfer rescues hearing in a mouse model of hereditary deafness. Hum. Mol. Genet. **24**, 3651–3661 (2015). 10.1093/hmg/ddv109
25. Qi, J., et al.: AAV gene therapy for autosomal recessive deafness 9: a single-arm trial. Nat. Med. **31**, 2917–2926 (2025). 10.1038/s41591-025-03773-w
26. Qi, J., Xu, L., Zeng, F.G., Chai, R.: OTOF-related gene therapy: a new way but a long road ahead. Lancet (London England). **405**, 777–779 (2025). 10.1016/s0140-6736(25)00248-x
27. Lv, J., et al.: AAV1-hOTOF gene therapy for autosomal recessive deafness 9: a single-arm trial. Lancet (London England). (2024). 10.1016/s0140-6736(23)02874-x
28. Yoshimura, H., Shibata, S.B., Ranum, P.T., Moteki, H., Smith, R.J.H.: Targeted Allele Suppression Prevents Progressive Hearing Loss in the Mature Murine Model of Human TMC1 Deafness. Mol. Ther. **27**, 681–690 (2019). 10.1016/j.ymthe.2018.12.014
29. Gao, X., et al.: Treatment of autosomal dominant hearing loss by in vivo delivery of genome editing agents. Nature. **553**, 217–221 (2018). 10.1038/nature25164
30. Tao, Y., et al.: AAV-ie-K558R mediated cochlear gene therapy and hair cell regeneration. Signal. Transduct. Target. therapy. **7** (2022). 10.1038/s41392-022-00938-8
31. Xue, Y., et al.: Gene editing in a Myo6 semi-dominant mouse model rescues auditory function. Mol. Ther. **30**, 105–118 (2022). 10.1016/j.ymthe.2021.06.015
32. Guo, Y., et al.: Specific knockdown of Htra2 by CRISPR-CasRx prevents acquired sensorineural hearing loss in mice. Mol. Ther. Nucleic Acids. **28**, 643–655 (2022). 10.1016/j.omtn.2022.04.014
33. Pan, B., et al.: Gene therapy restores auditory and vestibular function in a mouse model of Usher syndrome type 1c. Nat. Biotechnol. **35**, 264–272 (2017). 10.1038/nbt.3801
34. Liu, L., et al.: Template-independent genome editing in the Pcdh15(av-3j) mouse, a model of human DFNB23 nonsyndromic deafness. Cell. Rep. **40**, 111061 (2022). 10.1016/j.celrep.2022.111061
35. Zhao, X., Liu, H., Liu, H., Cai, R., Wu, H.: Gene Therapy Restores Auditory Functions in an Adult Vglut3 Knockout Mouse Model. Hum. Gene Ther. **33**, 729–739 (2022). 10.1089/hum.2022.062

36. Zhang, H., et al.: Simultaneous zygotic inactivation of multiple genes in mouse through CRISPR/Cas9-mediated base editing. Dev. (Cambridge England). **145** (2018). 10.1242/dev.168906

Figures

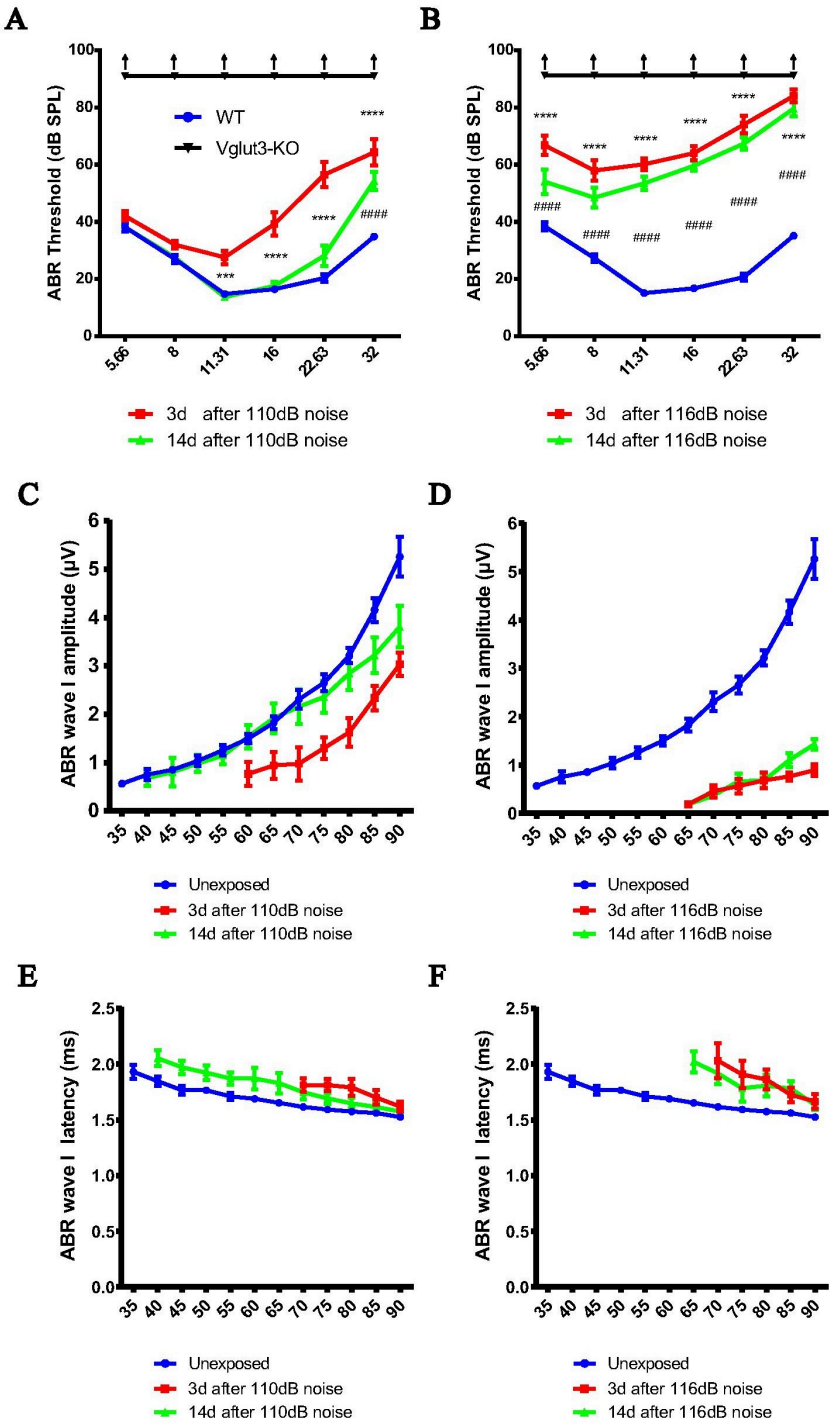


Figure 1

Noise exposure induces temporary and permanent threshold shifts in wild-type mice.

(A) Auditory brainstem response (ABR) threshold shifts in wild-type mice at 3 and 14 days following exposure to 110 dB SPL broadband noise (2–20 kHz, 2 hours), compared to unexposed controls. (B) ABR threshold shifts in wild-type mice at 3 and 14 days following exposure to 116 dB SPL broadband noise under the same conditions. (C, D) Quantification of ABR wave I amplitudes at 22.63 kHz in response to 90 dB SPL click stimuli before and after noise exposure at 110 dB (C) and 116 dB (D). (E, F) Quantification of ABR wave I latencies at 22.63 kHz in response to 90 dB SPL click stimuli before and after noise exposure at 110 dB (E) and 116 dB (F). Data are presented as mean ± SEM.

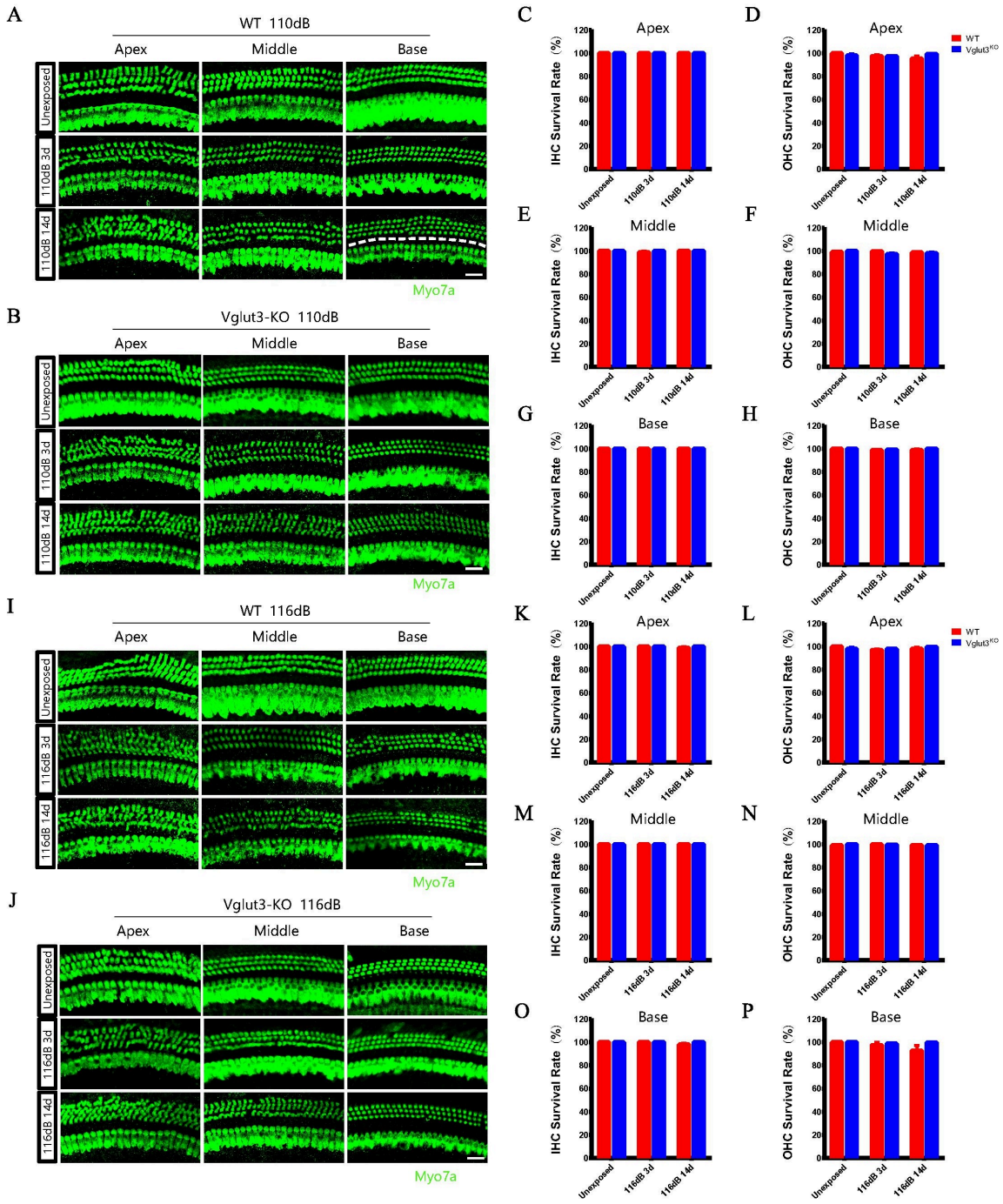


Figure 2

Hair cell survival in wild-type and Vglut3-KO mice following noise exposure.

(A, B, I, J) Representative confocal images of cochlear whole mounts immunostained for Myo7a (green) to label inner and outer hair cells in the apical, middle, and basal turns. (C - H) Quantification of inner and outer hair cell survival across all cochlear turns in wild-type and Vglut3-KO mice exposed to 110 dB SPL

broadband noise. (K - P) Quantification of inner and outer hair cell survival across all cochlear turns in wild-type and Vglut3-KO mice exposed to 116 dB SPL broadband noise. Data are presented as mean ± SEM. Scale bars: 20 µm.

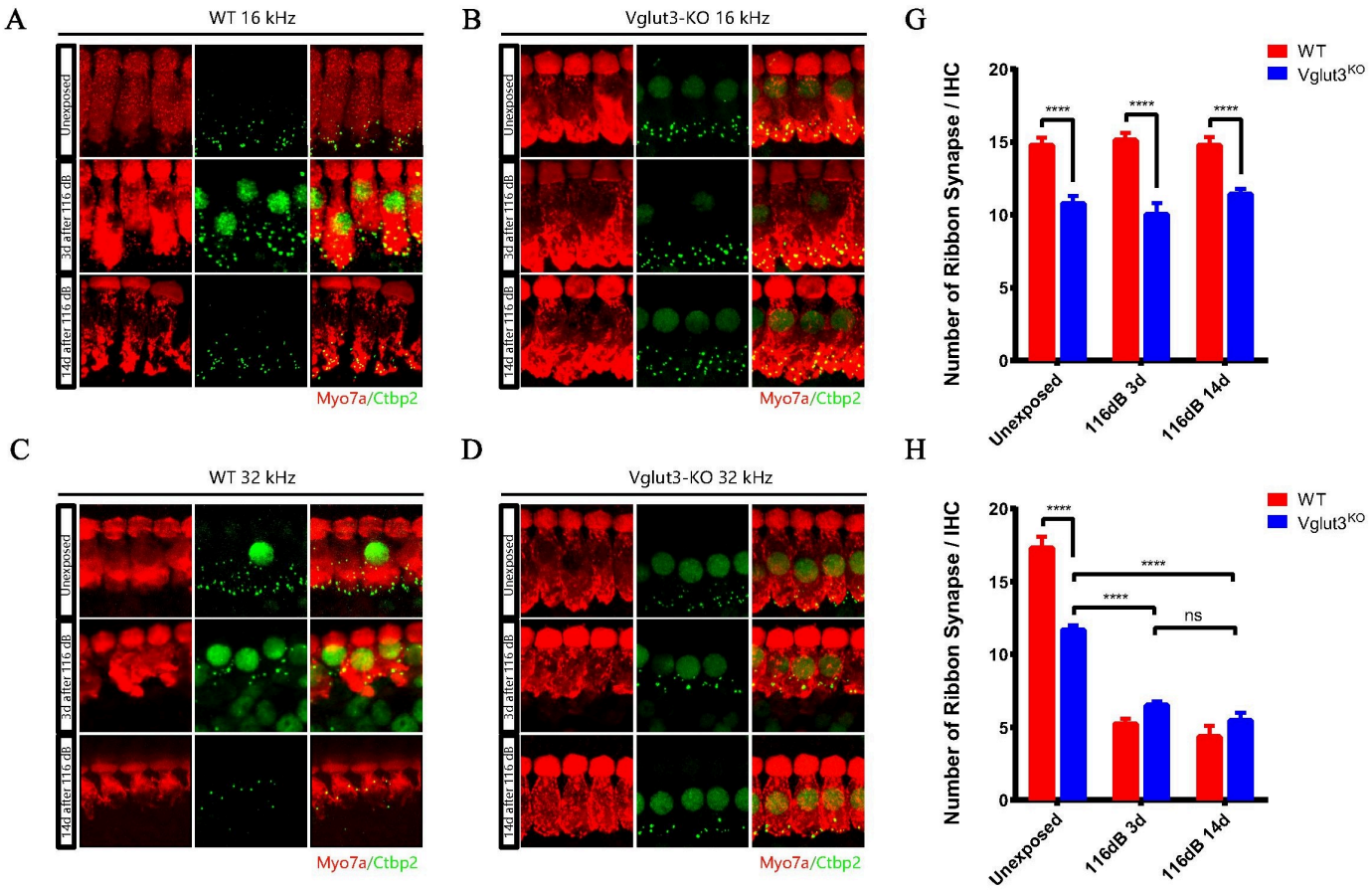


Figure 3

Noise-induced synaptopathy in wild-type and Vglut3-KO mice.

(A-D) Representative confocal images of cochlear whole mounts from the indicated genotypes and experimental groups, immunostained for CtBP2 (green) to label presynaptic ribbons in inner hair cells at the 16 kHz and 32 kHz cochlear regions. (E) Quantification of ribbon synapses per inner hair cell in the 16 kHz region of wild-type and Vglut3-KO mice at 3 and 14 days following exposure to 116 dB SPL broadband noise, compared to unexposed controls. (F) Quantification of ribbon synapses per inner hair cell in the 32 kHz region of wild-type and Vglut3-KO mice at 3 and 14 days following exposure to 116 dB SPL broadband noise, compared to unexposed controls. Data are presented as mean ± SEM. Scale bars: 10 µm.

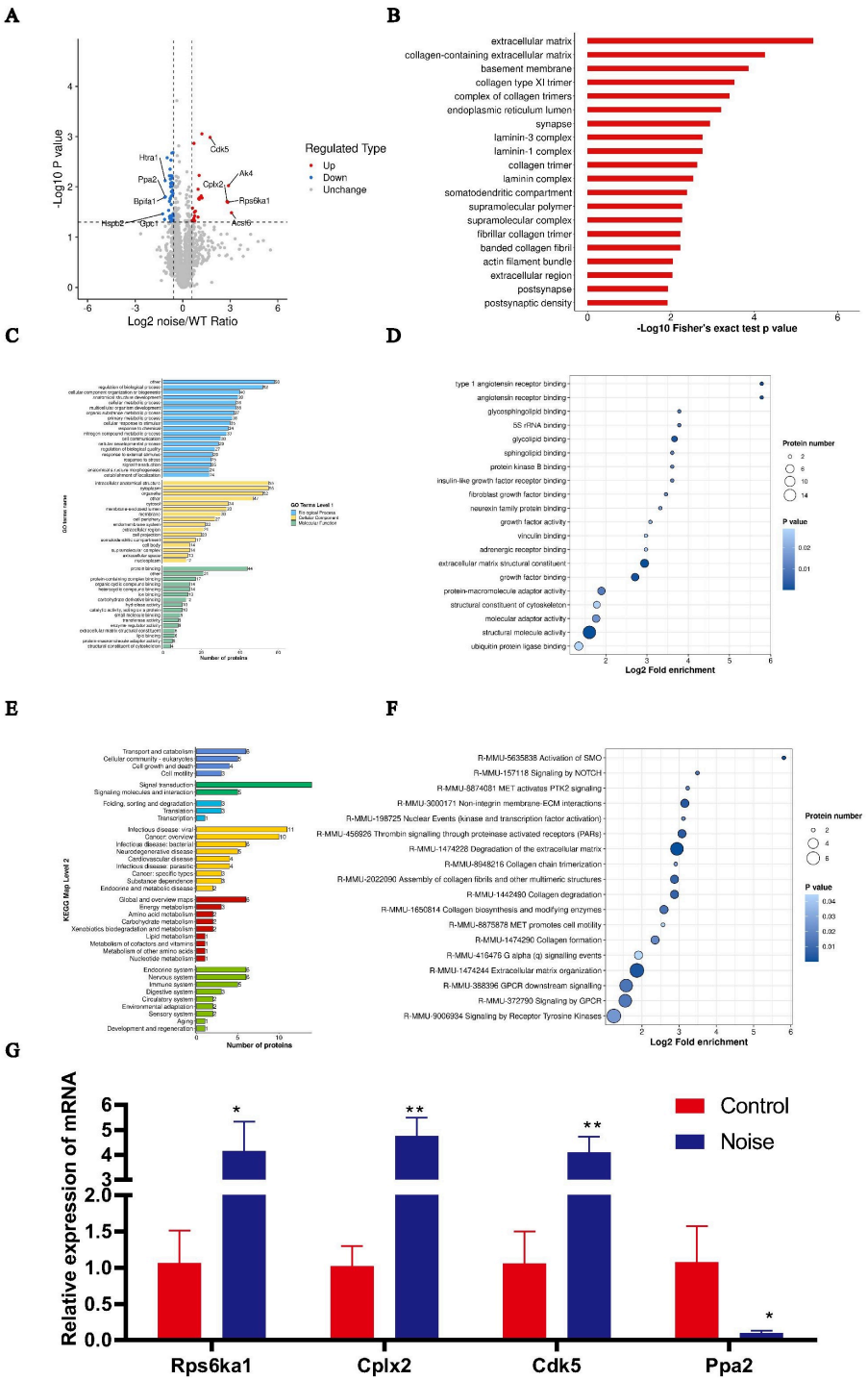


Figure 4

Proteomic profiling reveals synaptic and extracellular matrix disruption following noise exposure.

(A) Volcano plot illustrating differentially expressed proteins (DEPs) in cochlear extracts from wild-type mice following 116 dB SPL noise exposure, with significantly upregulated (red) and downregulated (blue) proteins indicated. (B) Gene Ontology (GO) cellular component enrichment analysis of DEPs, highlighting

significantly enriched synaptic and extracellular matrix terms. (C) GO biological process enrichment analysis of DEPs following noise exposure. (D) GO molecular function enrichment analysis of DEPs, showing significantly enriched terms related to synaptic signaling, lipid binding, and cell adhesion. (E) KEGG pathway enrichment analysis of DEPs, categorized by major functional classes. (F) Reactome pathway enrichment analysis of DEPs, revealing significant enrichment of extracellular matrix organization and signaling pathways. (G) Validation of selected DEPs by quantitative PCR, confirming transcriptional changes in key synaptic and extracellular matrix genes. Data are presented as mean ± SEM.

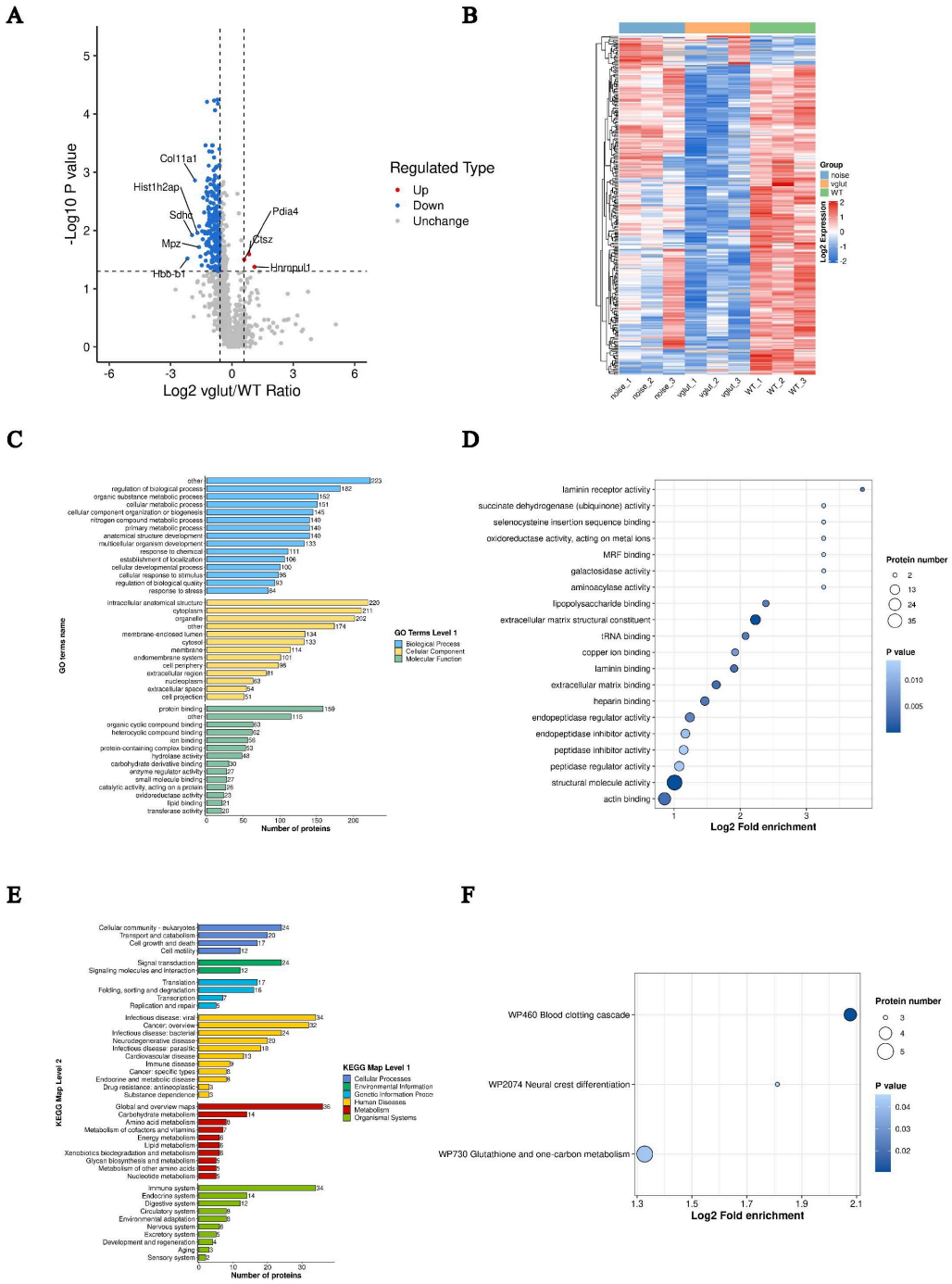


Figure 5

Proteomic profiling of Vglut3 knockout mice reveals extensive synaptic and metabolic alterations.

(A) Volcano plot illustrating differentially expressed proteins (DEPs) in cochlear extracts from Vglut3 knockout mice compared to wild-type controls, with significantly upregulated (red) and downregulated (blue) proteins indicated. (B) Hierarchical clustering analysis showing distinct separation of proteomic

profiles between wild-type and Vglut3 knockout samples. (C) Gene Ontology (GO) cellular component enrichment analysis of DEPs in Vglut3 knockout mice, highlighting significantly enriched synaptic, mitochondrial, and extracellular matrix terms. (D) GO molecular function enrichment analysis of DEPs, showing significantly enriched terms related to synaptic transmission, ion channel activity, and energy metabolism. (E) KEGG pathway enrichment analysis of DEPs, categorized by major functional classes. (F) WikiPathways enrichment analysis of DEPs, revealing significant enrichment of synaptic function, mitochondrial energy metabolism, and extracellular matrix pathways. Data are presented as mean ± SEM.

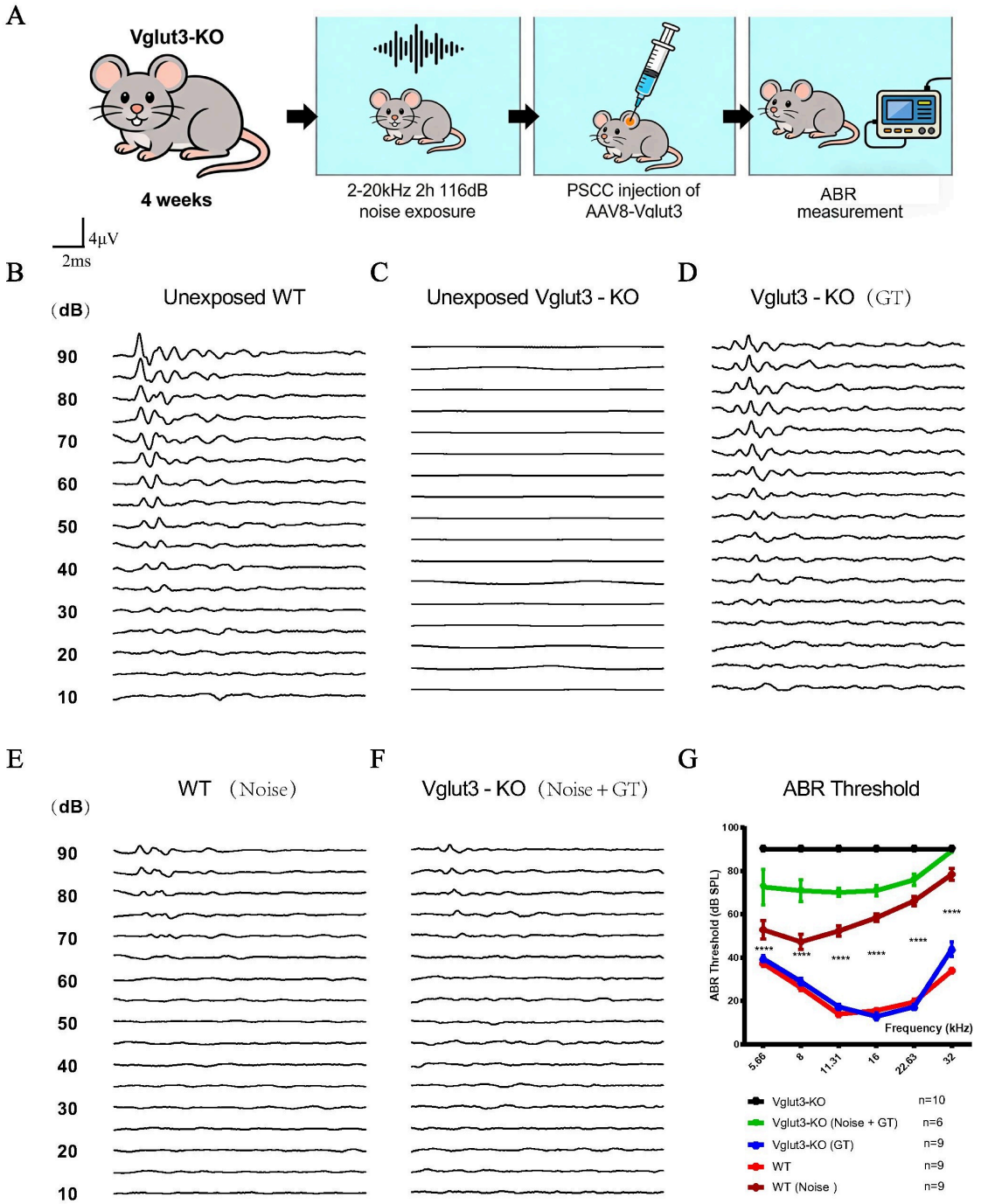


Figure 6

Noise exposure compromises gene therapy efficacy in Vglut3 knockout mice.

(A) Representative ABR waveforms at 16 kHz recorded from wild-type mice, showing normal auditory responses. (B) Representative ABR waveforms at 16 kHz recorded from untreated Vglut3 knockout mice, demonstrating absent auditory responses. (C) Representative ABR waveforms at 16 kHz recorded from

Vglut3 knockout mice following AAV8-Vglut3 gene therapy via posterior semicircular canal injection, showing restoration of auditory function. (D) Representative ABR waveforms at 16 kHz recorded from wild-type mice 14 days after exposure to 116 dB SPL broadband noise. (E) Representative ABR waveforms at 16 kHz recorded from Vglut3 knockout mice 14 days after exposure to 116 dB SPL broadband noise, followed by AAV8-Vglut3 gene therapy and assessed 14 days post-treatment. (F) Quantification and comparison of ABR thresholds across all tested frequencies (5.66, 8, 11.31, 16, 22.63, and 32 kHz) for the conditions depicted in panels A-E. Data are presented as mean ± SEM. Scale bars in (A-E): 2 ms (horizontal), 4 μV (vertical).

Supplementary Files

This is a list of supplementary files associated with this preprint. Click to download.

- RS515.pdf
- SupplementaryFigure.docx